# Structures and Spectroscopic Properties of Bis(phthalocyaninato) Yttrium and Lanthanum Complexes: Theoretical Study Based on Density Functional Theory Calculations

**Yuexing Zhang,[†] Xue Cai,[†,‡] Yang Zhou,[†] Xianxi Zhang,[†,§] Hui Xu,[†] Zhongqiang Liu,[†] Xiyou Li,*[,†] and Jianzhuang Jiang*[,†]**

*Department of Chemistry, Shandong University, Jinan 250100, China, Department of Chemistry, Mudanjiang Teacher's College, Mudanjiang 157012, China, and School of Chemistry and Chemical Engineering, Liaocheng University, Liaocheng 252059, China*

*Received: September 20, 2006; In Final Form: October 26, 2006*

Density functional theory (DFT) calculations were carried out to describe the molecular structures, molecular orbitals, atomic charges, UV−vis absorption spectra, IR, and Raman spectra of bis(phthalocyaninato) rare earth(III) complexes $M(Pc)_2$ (M = Y, La) as well as their reduced products $[M(Pc)_2]^-$ (M = Y, La). Good consistency was found between the calculated results and experimental data. Reduction of the neutral $M(Pc)_2$ to $[M(Pc)_2]^-$ induces the reorganization of their orbitals and charge distribution and decreases the inter-ring interaction. With the increase of ionic size from Y to La, the inter-ring distance of both the neutral and reduced double-decker complexes $M(Pc)_2$ and $[M(Pc)_2]^-$ (M = Y, La) increases, the inter-ring interaction and splitting of the Q bands decrease, and corresponding bands in the IR and Raman spectra show a red shift. The orbital energy level and orbital nature of the frontier orbitals are also described and explained in terms of atomic character. The present work, representing the first systemic DFT study on the bis(phthalocyaninato) yttrium and lanthanum complexes sheds further light on clearly understanding structure and spectroscopic properties of bis(phthalocyaninato) rare earth complexes.

## Introduction

Phthalocyanines are an important class of pigments that have fascinated scientists for many years because of their applications in various disciplines.[1] It is also well-known that phthalocyanines can form sandwich-type complexes with a range of metal ions, including rare earths, actinides, early transition metals, and some main-group metals.[2,3] The resulting bis(phthalocyaninato) metal complexes, especially the rare earth double-deckers, possess intriguing and unique electronic and optical properties that make them useful in materials science associated with their potential applications in molecular electronics, nonlinear optics, sensors, and optically addressed spatial light modulators.[4−7]

Research results reported thus far have revealed that the electrochemical and spectroscopic properties of bis(phthalocyaninato) rare earth double-decker complexes are closely related to the inter-ring distance in the molecule, which is determined by the ionic size of the central rare earth metal and the strength of the metal−ligand bonds.[8−12] However, a fundamental understanding of the relationships among the conjugated Pc ring, central metal, peripheral and/or nonperipheral substituents, the molecular geometry, and the spectroscopic and electrochemical properties is still absent in this research field. In spite of reports on theoretical studies of the electronic absorption and NMR spectra as well as the magnetic properties of some bis(phthalocyaninato) and tris(phthalocyaninato) rare earth complexes by Ishikawa et al.,[13] efforts toward understanding the spectroscopic and electrochemical properties of sandwich-type phthalocyaninato rare earth complexes through theoretical study have been retarded due to the large molecular system of these compounds and, in particular, the well-known difficulties in doing calculations on the system involving the f-electron-containing metal element. Thus selection of bis(phthalocyaninato) complexes of rare earth metals including non-f-electron-containing tervalent yttrium and lanthanum renders it possible to do theoretical calculations at this stage.[14]

In recent years, along with the development of computer industry and calculation method, calculations and simulations on large molecular and even supramolecular systems with more than 100 atoms have become possible. Density functional theory (DFT) methods, at the B3LYP level,[15] have proved suitable for the energy-minimized structure and property calculations for both metal-free and metallo phthalocyanines,[16−19] and meanwhile the Los Alamos National Laboratory (LANL2DZ) effective core pseudopotentials[20] with D95 on first row,[21] Los Alamos ECP plus DZ on Na−Bi basis set, proved appropriate for studying metal complexes with central metals having a large atomic number.[14,17,18,22] However, there is still no appropriate basis set to study all the rare earth metals due to the complicated f electrons. As a result, only the compounds of yttrium and lanthanum are selected in this study.

In this paper, we studied the molecular structures, molecular orbitals, atomic charges, and UV−vis, IR, and Raman spectra of neutral bis(phthalocyaninato) rare earth(III) complexes $M(Pc)_2$ (M = Y, La) as well as their reduced products $[M(Pc)_2]^-$ (M = Y, La), by the density functional theory (DFT) method at the B3LYP level with LANL2DZ basis set. Good consistency between the calculated results and experimental data demonstrates the good performance of this method for such bis(phthalocyaninato) rare earth systems. To the best of our knowledge, this appears to represent the first effort toward

* Corresponding author: e-mail jzjiang@sdu.edu.cn.
[†] Shandong University.
[‡] Mudanjiang Teacher's College.
[§] Liaocheng University.

10.1021/jp066157g CCC: $37.00 
Published on Web 12/15/2006

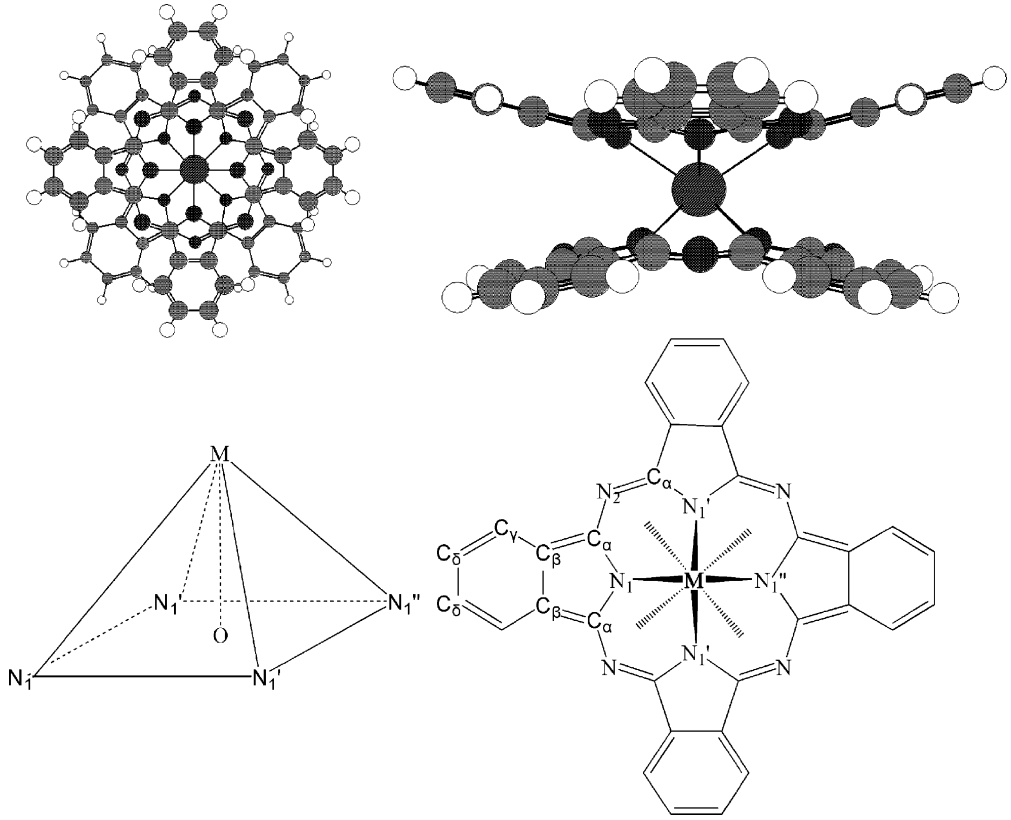


**Figure 1.** Optimized structures (top) and atomic labeling (bottom) of $Y(Pc)_2$. The label O is the center of the square formed by four isoindole nitrogen atoms.

understanding the structures and spectroscopic properties of bis(phthalocyaninato) yttrium and lanthanum complexes by DFT calculations.

## Experimental and Computational Details

Bis(phthalocyaninato) rare earth complexes $M(Pc)_2$ (M = Y, La) were prepared according to published procedure.[23] Electronic absorption spectra were recorded at room temperature on a Hitachi U-4100 spectrophotometer in chloroform. IR spectra were recorded for KBr pellets on a Bio-Rad FTS-165 spectrometer in the range of 4000−400 $cm^{-1}$ with resolution of 2 $cm^{-1}$.

The primary input structure of $M(Pc)_2$ (M = Y, La) was obtained by putting yttrium and lanthanum atoms into the center of two parallel phthalocyanine rings, in which the distance between the two Pc rings was set to 3.0 Å and one Pc ring was rotated 45° around the axis, passing through the rare earth atom and perpendicular to the Pc rings. The hybrid density functional B3LYP (Becke−Lee−Young−Parr composite of exchange-correlation functional) method was used for both geometry optimizations and property calculations.[15] In all cases, the LANL2DZ basis set was used.[20,21] The Berny algorithm using redundant internal coordinates was employed in energy minimization and the default cutoffs were used throughout.[24] $D_{4d}$ symmetry for all the complexes in the input structures was detected and then enforced by the program. By use of the energy-minimized structures generated in the previous step, normal coordinate analyses were carried out. Charge distribution is carried out by a full natural bond orbital analysis (NBO) population method based on the minimized structure. The primarily calculated vibrational frequencies were scaled by the factor 0.9614.[25] UV−vis spectroscopic calculations were made by a time-dependent (TD) DFT method. All calculations were carried out with the Gaussian 03 program[26] in the IBM P690 system in Shandong Province High Performance Computing Center.

## Results and Discussion

**Molecular Structures.** The energy-minimized structures optimized at the B3LYP/LANL2DZ level all show $D_{4d}$ symmetry for both the neutral and reduced forms of bis(phthalocyaninato) rare earth complexes $M(Pc)_2$ and $[M(Pc)_2]^-$ (M = Y, La). For all these complexes, the metal atoms are sandwiched between two phthalocyanine (Pc) rings, which are distorted to dishlike shapes and are rotated relative to the other by 45°, and the central metal has square antiprism coordination geometry formed by eight isoindole nitrogen atoms ($N_1$). It is noteworthy that no imaginary vibration is predicted in the following frequency calculations of the IR and Raman vibrational spectroscopy, which indicates that the energy-minimized structures for all of the four complexes are true energy minima.

Figure 1 shows the optimized structures and atomic labeling of $Y(Pc)_2$, and Table 1 lists the structural parameters of all the complexes compared with experimental data available.[23,27−29] As can be found, the structural parameters of our minimum-energy geometry are in good accord with the experimental values.[23,27−29] The largest difference of bond length between our calculated data and the experimental results is revealed to be only 0.07 Å for the La−N bond of $La(Pc)_2$, and the smallest is only 0.01 Å for the $C_\beta-C_\gamma$ bond of $[Y(Pc)_2]^-$. The largest difference for bond angle, between the present calculated data and experimental results, is found for $\angle C_\alpha N_2 C_\alpha$ of $La(Pc)_2$, which is only 2.6°. This slightly larger bond angle difference between the calculated and experimental results is then responsible for the somewhat larger difference of the distance between two adjacent isoindole nitrogen atoms, a bit larger than 0.1 Å.

**TABLE 1: Calculated and Experimental Main Structure Parameters of $Y(Pc)_2$, $[Y(Pc)_2]^-$, $La(Pc)_2$, and $[La(Pc)_2]^-$**

| parameter[a] | $Y(Pc)_2$[b] | $[Y(Pc)_2]^-$ [b] | $La(Pc)_2$[b] | $[La(Pc)_2]^-$ [b] | $Y(Pc)_2\cdot CH_2Cl_2$[c] | $(n\text{-}Bu)_4N\cdot[Y(Pc^{2-})_2]$[d] | $La(Pc)_2\cdot CH_2Cl_2$[e] | $(PNP)[La(Pc^{2-})_2]$[f] |
|---|---|---|---|---|---|---|---|---|
| $MN_1$ | 2.449 | 2.463 | 2.586 | 2.602 | 2.400 | 2.408 | 2.515 | 2.554 |
| $N_1C_\alpha$ | 1.390 | 1.390 | 1.389 | 1.389 | 1.368 | 1.374 | 1.368 | 1.375 |
| $C_\alpha C_\beta$ | 1.474 | 1.471 | 1.478 | 1.474 | 1.465 | 1.458 | 1.426 | 1.462 |
| $C_\beta C_\beta$ | 1.416 | 1.418 | 1.420 | 1.421 | 1.389 | 1.388 | 1.390 | 1.367 |
| $C_\beta C_\gamma$ | 1.400 | 1.403 | 1.400 | 1.403 | 1.390 | 1.404 | 1.388 | |
| $C_\gamma C_\delta$ | 1.411 | 1.408 | 1.411 | 1.408 | 1.392 | 1.372 | 1.380 | |
| $C_\delta C_\delta$ | 1.417 | 1.420 | 1.416 | 1.419 | 1.383 | 1.399 | 1.383 | 1.386 |
| $C_\alpha N_2$ | 1.342 | 1.342 | 1.346 | 1.346 | 1.330 | 1.328 | 1.340 | 1.321 |
| $C_\gamma H_\alpha$ | 1.086 | 1.086 | 1.086 | 1.086 | 0.951 | 0.930 | | |
| $C_\delta H_\beta$ | 1.087 | 1.088 | 1.087 | 1.088 | 0.952 | 0.930 | | |
| MO[a] | 1.366 | 1.384 | 1.554 | 1.575 | 1.380 | 1.388 | 1.553 | 1.598 |
| $\angle N_1N_1'$ | 2.874 | 2.882 | 2.923 | 2.928 | 2.778 | 2.783 | 2.799 | 2.817 |
| $\angle N_1MN_1$ | 71.87 | 71.61 | 68.83 | 68.49 | 70.70 | 70.59 | 67.60 | 66.95 |
| $\angle N_1MN_1$ | 112.2 | 111.7 | 106.1 | 105.5 | 109.8 | 109.6 | 103.7 | 102.5 |
| $\angle C_\alpha N_1 C_\alpha$ | 108.0 | 108.0 | 108.9 | 109.0 | 108.0 | 107.7 | 108.2 | 109.0 |
| $\angle N_1 C_\alpha C_\beta$ | 109.5 | 109.4 | 108.9 | 108.8 | 109.6 | 109.5 | 109.5 | 108.2 |
| $\angle C_\alpha C_\beta C_\beta$ | 106.4 | 106.4 | 106.5 | 106.5 | 106.3 | 106.5 | 106.4 | 106.8 |
| $\angle C_\alpha C_\beta C_\gamma$ | 132.2 | 132.4 | 132.2 | 132.4 | 132.1 | 132.8 | | 131.1 |
| $\angle C_\beta C_\beta C_\gamma$ | 121.3 | 121.2 | 121.2 | 121.1 | 121.5 | 120.6 | 121.0 | 121.7 |
| $\angle C_\beta C_\gamma C_\delta$ | 117.6 | 117.8 | 117.7 | 117.9 | 116.7 | 118.1 | 117.6 | 115.6 |
| $\angle C_\gamma C_\delta C_\delta$ | 121.1 | 121.0 | 121.0 | 121.0 | 121.6 | 121.2 | 121.4 | 122.8 |
| $\angle N_1 C_\alpha N_2$ | 127.6 | 127.7 | 127.6 | 127.7 | 127.9 | 127.8 | 127.5 | 127.8 |
| $\angle N_2 C_\alpha C_\beta$ | 122.7 | 122.6 | 123.2 | 123.1 | 122.5 | 122.5 | | 123.8 |
| $\angle C_\alpha N_2 C_\alpha$ | 125.0 | 125.1 | 126.1 | 126.2 | 122.7 | 123.0 | 123.5 | 124.4 |
| $\angle MN_1N_1$ | 33.9 | 34.2 | 36.9 | 37.3 | 35.1 | 35.2 | 38.1 | 38.7 |
| $C_\delta$ deviation from $N_1$ plane | 1.189 277 | 1.262 054 | 1.270 924 | 1.314 881 | | | | |

[a] See Figure 1 for atomic labeling. [b] Calculated data. [c] Experimental data taken from ref 23. [d] Experimental data taken from ref 27. [e] Experimental data taken from ref 28. [f] Experimental data taken from ref 29.

The calculated distance of yttrium/lanthanum atom to the plane formed by four isoindole nitrogen atoms of the Pc ring is only 0.023 Å shorter compared with that observed by X-ray single crystal analysis. Good consistency between our calculated structural parameters and the X-ray single-crystal analysis data for both the neutral and reduced species of double-decker complexes clearly indicates that the method and basis set chosen here are suitable for calculations on bis(phthalocyaninato) rare earth(III) systems.

Introducing one electron to the semioccupied HOMO of neutral species $M(Pc)_2$ (M = Y, La) and thus changing it to a closed-shell system $[M(Pc)_2]^-$ induces many change in the structures according to the calculated results (Table 1). For example, for the yttrium complexes, both the Y−N bond length and the inter-ring distance in $[Y(Pc)_2]^-$ are longer compared with those in $Y(Pc)_2$, indicating that the inter-ring $\pi-\pi$ interaction in $[Y(Pc)_2]^-$ is weaker than that in $Y(Pc)_2$. However, the structural differences between $[Y(Pc)_2]^-$ and $Y(Pc)_2$ are still not very significant, which is clearly revealed by the largest differences between $[Y(Pc)_2]^-$ and $Y(Pc)_2$ for Y−N bond length and $\angle N_1MN_1$ bond angle, 0.01 Å and 0.3°, respectively. However, according to our calculations, the deviation of the outermost carbon atoms ($C_\delta$) from the mean plane formed by the four isoindole nitrogen atoms in $Y(Pc)_2$ is 0.07 Å smaller than in $[Y(Pc)_2]^-$. This is in line with the result of Ostendorp and Homborg[28] that Pc ligand in bis(phthalocyaninato) metal complexes tends to become planar upon oxidation.

The ionic radius of $La^{3+}$ is about 0.17 Å bigger than $Y^{3+}$; thus the structure parameters of $La(Pc)_2$ and $[La(Pc)_2]^-$ should have significant differences compared with those of $Y(Pc)_2$ and $[Y(Pc)_2]^-$. When the neutral complexes are compared, for example (Table 1), the La−N bond length is about 0.14 Å longer than the Y−N bond length, and the inter-ring distance in $La(Pc)_2$ is about 0.38 Å bigger than in $Y(Pc)_2$. This indicates that the inter-ring $\pi-\pi$ interaction in $La(Pc)_2$ is weaker than that in $Y(Pc)_2$. This is also true for the reduced double-decker complexes (Table 1). However, the structure parameters of the two Pc rings in both compounds change little. For the deviation of $C_\delta$ from the $N_1$ plane, a deviation of more than 1.27 Å is found in $La(Pc)_2$, which is about 0.08 Å bigger than that of $Y(Pc)_2$.

It is noteworthy again that the calculated results in the structures of bis(phthalocyaninato) rare earth complexes $M(Pc)_2$ (M = Y, La) show that along with the increase in ionic size from Y to La, all the following structural parameters including the M−N bond length, inter-ring distance, and deviation of the outermost carbon atoms from the mean plane formed by the four isoindole nitrogen atoms increase significantly. In contrast, both the bond lengths and bond angles within the two Pc rings of the double-decker molecules change little. This is also true for the reduced double-deckers $[M(Pc)_2]^-$ (M = Y, La) on the basis of present calculations and actually is in line with the experimental fundings.[23,27−29]

**Molecular Orbitals.** Both $Y(Pc)_2$ and $La(Pc)_2$ have an unpaired electron, and they have the same ground electronic state of $^2A_2$ with a spin multiplicity of 2. Unrestricted DFT method was used for the calculation of these open-shell systems. In contrast, the two reduced compounds $[Y(Pc)_2]^-$ and $[La(Pc)_2]^-$ have the electronic state of $^1A_1$ due to the closed-shell systems without unpaired electrons. Figure 2 compares the calculated molecular orbital energy levels of $Y(Pc)_2$, $[Y(Pc)_2]^-$, $La(Pc)_2$, and $[La(Pc)_2]^-$ together with their orbital symmetry.

For $Y(Pc)_2$, the highest occupied molecular orbital (HOMO) is $\alpha$ $a_2$ orbital and the lowest unoccupied molecular orbital (LUMO) is $\beta$ $a_2$ orbital, and the HOMO−LUMO energy gap is 0.84 eV, which is much lower than the energy gap between the $\alpha$ $a_2$ orbital (HOMO) and the $\alpha$ $e_3$ orbital (the lowest unoccupied $\alpha$ orbital) (1.87 eV). As a result, the added electron would occupy the $\beta$ $a_2$ orbital (LUMO) when $Y(Pc)_2$ is reduced to $[Y(Pc)_2]^-$. However, addition of one electron into the $\beta$ $a_2$ orbital

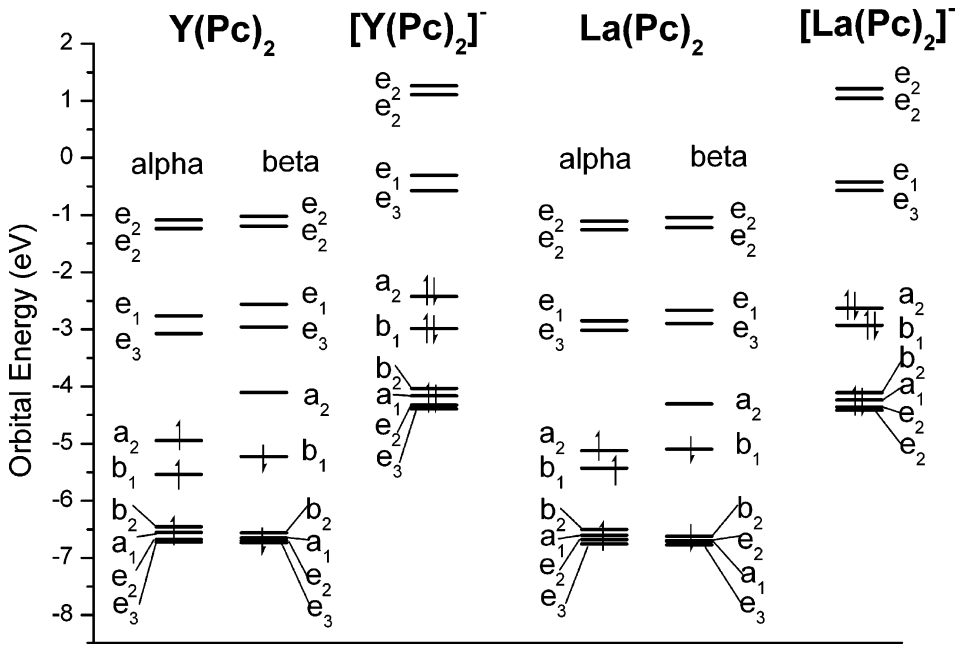


**Figure 2.** Calculated molecular orbital energy levels and symmetry of $Y(Pc)_2$, $[Y(Pc)_2]^-$, $La(Pc)_2$, and $[La(Pc)_2]^-$.

(LUMO) of $Y(Pc)_2$ then induces reorganization of all the molecular orbitals and the formation of the $^1A_1$ state closed-shell system in $[Y(Pc)_2]^-$. In $[Y(Pc)_2]^-$, the $a_2$ orbital becomes the HOMO, and the $e_3$ orbital becomes the LUMO, with the HOMO−LUMO energy gap increases to 1.85 eV, which is a little smaller compared with the energy gap between the α $a_2$ and $e_3$ orbitals. It is worth noting that the orbital energy order and symmetry in $[Y(Pc)_2]^-$ are the same as those in $Y(Pc)_2$; however, the energy level of the former is much higher than the latter due to the re-pairing of α and $\beta$ orbital. This result is consistent with the analysis in the Molecular Structures section, that is, the inter-ring distance in $[Y(Pc)_2]^-$ is longer than that in $Y(Pc)_2$ and the interaction between the two phthalocyanine rings of the former is weaker than the latter.

When the tervalent lanthanum ion with larger ionic size is introduced into the bis(phthalocyaninato) rare earth system, the $\beta$ $b_1$ orbital, instead of the α $a_2$ orbital in $Y(Pc)_2$, becomes the HOMO in $La(Pc)_2$ with the $\beta$ $a_2$ orbital remaining the LUMO. The HOMO−LUMO energy gap is 0.79 eV, about 0.05 eV lower than the HOMO−LUMO energy gap of $Y(Pc)_2$. However, the energy gap between the α $a_2$ occupied orbital and the α $e_3$ unoccupied α orbital, 2.11 eV, is much larger than the corresponding gap for $Y(Pc)_2$. As clearly displayed in Figure 2, the energy of the α $a_2$ orbital for $La(Pc)_2$ decreases to a large degree compared with that for $Y(Pc)_2$. This not only explains the larger energy gap between the α $a_2$ occupied orbital and the α $e_3$ unoccupied orbital but also forms the reason that the $\beta$ $b_1$ orbital in $La(Pc)_2$ becomes the HOMO. It is noteworthy that the α frontier orbitals of $La(Pc)_2$ have the same energy order as those of $Y(Pc)_2$, but some of the $\beta$ frontier orbitals of $La(Pc)_2$ are in reverse energy order of $Y(Pc)_2$. Upon reduction of $La(Pc)_2$ into $[La(Pc)_2]^-$ by adding one electron into the semioccupied HOMO of the neutral molecule, reorganization of molecular orbitals also takes place and the HOMO ($a_2$)−LUMO ($e_3$) energy gap is revealed to be 2.06 eV according to the calculation results. This value is larger than that for both $La(Pc)_2$ and $[Y(Pc)_2]^-$, indicating weaker interaction between the two phthalocyanine rings of $[La(Pc)_2]^-$ compared with that in $La(Pc)_2$ and $[Y(Pc)_2]^-$ due to the larger inter-ring distance. It is worth mentioning that the larger HOMO−LUMO gap for $[La(Pc)_2]^-$ compared with that for $[Y(Pc)_2]^-$ revealed by the present calculations is in good agreement with that revealed by electrochemical measurements for these complexes.[30]

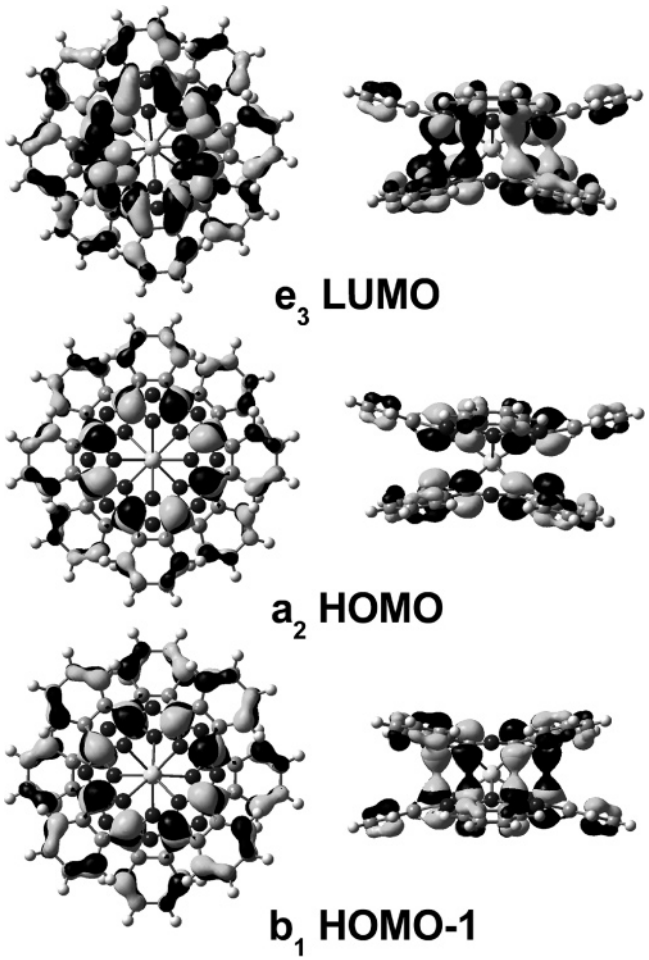


**Figure 3.** α Molecular orbital map of $Y(Pc)_2$ (left, top view; right, side view).

The molecular orbital map of the α orbitals of $Y(Pc)_2$ is shown in Figure 3 and Figure S1 (Supporting Information), and the atomic composition of the molecular orbitals from HOMO

− 2 to LUMO of $Y(Pc)_2$, $[Y(Pc)_2]^-$, $La(Pc)_2$, and $[La(Pc)_2]^-$ are listed in Table S1 (Supporting Information). It is worth noting that all the orbitals of the remaining complexes $[Y(Pc)_2]^-$, $La(Pc)_2$, and $[La(Pc)_2]^-$ have very similar appearance to the corresponding orbitals of $Y(Pc)_2$ despite the different orbital energy levels. The α HOMO (270 $a_2$ orbital) of $Y(Pc)_2$ is mainly composed of $4p_z$ and $5p_z$ orbitals of $C_\alpha$ atoms and $4p_z$ orbitals of $C_\gamma$ and $C_\delta$ atoms. As can be seen from Figures 3 and S1 (Supporting Information), the $p_z$ orbitals of the neighboring $C_\alpha$ atoms in each Pc ring and different Pc rings are opposite in direction. There is no bonding interaction between the $p_z$ atomic orbitals of $C_\alpha$ due to their unsuitable distance and orientation. It is noteworthy that despite the smaller contribution of $C_\gamma$ and $C_\delta$ atoms to the α HOMO than $C_\alpha$ atoms, the formation of $\pi$ orbital between the adjacent $4p_z$ orbital of $C_\gamma$ and $C_\delta$ in each isoindole makes this $a_2$ molecular orbital stable. The more orbital composition is distributed to $C_\gamma$ and $C_\delta$ atoms, the more stable the molecular orbital is. The α HOMO−1 (269 $b_1$) orbital of $Y(Pc)_2$ is also made up of the $4p_z$ and $5p_z$ orbitals of $C_\alpha$ atoms and $4p_z$ orbitals of $C_\gamma$ and $C_\delta$ atoms as the HOMO. However, the $4p_z$ and $5p_z$ orbitals of neighboring $C_\alpha$ atoms between two Pc rings can form a weak $\sigma$ bond, which makes the $b_1$ orbital much more stable than the $a_2$ orbital. Taking the atomic composition on one Pc ring as a whole segment, the α 270 $a_2$ orbital can be considered as the antibonding orbital between the two Pc rings in $Y(Pc)_2$, whereas the 269 $b_1$ orbital is the bonding orbital. The energy difference between 270 $a_2$ and 269 $b_1$ orbitals then reflects the interaction intensity between the two Pc rings in bis(phthalocyaninato) rare earth double-decker complexes. For example, the energy difference between 270 $a_2$ and 269 $b_1$ orbitals in both the neutral and reduced bis(phthalocyaninato) yttrium complexes is larger than in the lanthanum analogues, indicating stronger inter-ring interaction of the former than the latter. This is in accordance with the trend found in the Molecular Structures section.

As discussed above and organized in Table S1 (Supporting Information), the atomic composition and appearance of the molecular orbitals of $[Y(Pc)_2]^-$, $La(Pc)_2$, and $[La(Pc)_2]^-$ are similar to those of $Y(Pc)_2$ with the same symmetry, and the α and $\beta$ orbitals in $Y(Pc)_2$ and $La(Pc)_2$ are also very similar. As a consequence, the difference in orbital energy level of different complexes can be explained in term of different atomic composition of corresponding molecular orbitals. For example, due to the decreasing contribution of $4p_z$ and $5p_z$ orbitals of $C_\alpha$ atoms to the whole molecular orbital and the increasing contribution of $4p_z$ orbitals of $C_\gamma$ and $C_\delta$ atoms compared with that of $Y(Pc)_2$, the energy of α 270 $a_2$ orbital of $La(Pc)_2$ is much lower than that of $Y(Pc)_2$. In contrast, the α 269 $b_1$ orbital of $La(Pc)_2$ stands at a higher energy level than the corresponding orbital of $Y(Pc)_2$ because of the larger distribution of $p_z$ orbitals of $C_\alpha$ atoms and smaller distribution of $4p_z$ orbitals of $C_\gamma$ and $C_\delta$ atoms of $La(Pc)_2$ on the α 269 $b_1$ orbital than that on $Y(Pc)_2$.

**Atomic Charges.** To find out the distribution of the added electron in reduced complexes, charge distribution calculations were carried out by a full natural bond orbital analysis (NBO) population method based on the minimized structures of $Y(Pc)_2$ and $[Y(Pc)_2]^-$. The calculated NBO charges of $Y(Pc)_2$ and $[Y(Pc)_2]^-$ are organized in Table 2. Comparison between the NBO charges of $Y(Pc)_2$ and $[Y(Pc)_2]^-$ shows that the positive charge on yttrium atom and the negative charge on $C_\gamma$, $C_\delta$, and the meso nitrogen atoms ($N_2$) increase when one electron is added to $Y(Pc)_2$, whereas the positive charge on $C_\alpha$ atoms and the negative charge on $C_\beta$ and the isoindole nitrogen atoms decrease. The increase of the positive charge on yttrium atom

**TABLE 2: Calculated NBO Charges of $Y(Pc)_2$ and $[Y(Pc)_2]^-$**

| atom | $Y(Pc)_2$ | $[Y(Pc)_2]^-$ |
|---|---|---|
| M | 2.052 | 2.059 |
| $N_1$ | −0.708 | −0.700 |
| $C_\alpha$ | 0.485 | 0.458 |
| $C_\beta$ | −0.070 | −0.065 |
| $C_\gamma$ | −0.173 | −0.185 |
| $C_\delta$ | −0.205 | −0.221 |
| $N_2$ | −0.536 | −0.537 |

is in line with the increase in the Y−N bond length along with the reduction of $Y(Pc)_2$ to $[Y(Pc)_2]^-$. It is worth noting that the charge on $C_\alpha$, $C_\gamma$, and $C_\delta$ atoms changes more than that on the other atoms when $Y(Pc)_2$ is reduced to $[Y(Pc)_2]^-$. This is consistent with the conclusion resulted from orbital analysis that the added electron would occupy the $\beta$ $a_2$ orbital (LUMO), which is mainly composed of $4p_z$ and $5p_z$ orbitals of $C_\alpha$ atoms and $4p_z$ orbitals of $C_\gamma$ and $C_\delta$ atoms, when $Y(Pc)_2$ is reduced to $[Y(Pc)_2]^-$. The increase of the negative charges on $C_\gamma$ and $C_\delta$ and the decrease of the positive charge on $C_\alpha$ along with the reduction indicates that the added one electron is actually distributed on these atoms instead of on the isoindole nitrogen atoms, which is further supported by the decrease of the negative charge on the isoindole nitrogen atoms. As a result, the interaction between the phthalocyanine ring and the central metal decreases from $Y(Pc)_2$ to $[Y(Pc)_2]^-$.

Despite the fact that NBO calculations are not achieved for the systems of $La(Pc)_2$ and $[La(Pc)_2]^-$, their charge distributions should be reasonably similar to those of $Y(Pc)_2$ and $[Y(Pc)_2]^-$, respectively, due to their great structural similarity.

**Electronic Absorption Spectra.** Most probably due to the complicated systems related to the unpaired electron in the HOMO of $M(Pc)_2$ (M = Y, La), calculations with the present method failed to determine the excited-state symmetry and give reasonable electronic absorption spectra for these neutral species of double-decker compounds (Figure S2, Supporting Information). In contrast, electronic absorption spectra for the reduced forms $[M(Pc)_2]^-$ (M = Y, La) were provided according to the calculations and corresponding data are tabulated in Table 3. Figure 4 compares the simulated and experimental electronic absorption spectra of $[Y(Pc)_2]^-$ and $[La(Pc)_2]^-$. Accordingly, two groups of absorption bands appear in the electronic absorption spectra of the reduced double-deckers: for instance, in the case of $[Y(Pc)_2]^-$, a B band at 334 nm and two Q bands at 627 and 696 nm, respectively. On the basis of our calculation results, the B band of $[Y(Pc)_2]^-$ at 359 nm, corresponding well with the experimental data at 334 nm, is mainly contributed by the $\pi \rightarrow \pi^*$ electronic transition from HOMO ($a_2$ symmetry) to the much higher unoccupied orbital (281 $e_1$ orbital). Meanwhile, three electronic transitions with very much complicated transfer natures in the region of 360−400 nm should also have some contribution to the B band of the reduced double-decker according to the calculations. The calculated band at 415 nm for $[Y(Pc)_2]^-$ is mainly due to the $\pi \rightarrow \pi^*$ electronic transition from HOMO − 2 ($b_2$ symmetry) to LUMO. As the electrons in HOMO − 2 ($b_2$ orbital) mainly distribute on nitrogen atoms, whereas in LUMO ($e_3$ orbital) the molecular orbital has much composition on $C_\alpha$ and $C_\beta$ atoms, the band at 415 nm for $[Y(Pc)_2]^-$ can therefore be attributed to the electron transfer from nitrogen to carbon atoms within the Pc ring. As for the two calculated Q bands of $[Y(Pc)_2]^-$ at 568 and 716 nm, which correspond to the observed absorption at 627 and 696 nm, respectively, the latter one in longer wavelength was revealed to be mainly due to the $\pi \rightarrow \pi^*$ electronic transition

**TABLE 3: Calculated Electronic Absorption Spectra of $[Y(Pc)_2]^-$ and $[La(Pc)_2]^-$**

| $[Y(Pc)_2]^-$ | | $[La(Pc)_2]^-$ | |
|---|---|---|---|
| wavelength,[a] nm | transitions[b] | wavelength,[a] nm | transitions[b] |
| 359 (0.03) [334] | 44% $270^{HOMO}a_2 \rightarrow 281e_1$* | 359 (0.02) [334] | 29% $263e_2 \rightarrow 273e_1$* |
| | 26% $265e_2 \rightarrow 274\ e_1$ | | 28% $263e_2 \rightarrow 274e_1$* |
| | 24% $267a_1 \rightarrow 273e_1$ | | |
| 386 (0.01) | 31% $265e_2 \rightarrow 272^{LUMO}e_3$* | 385 (0.02) | 36% $265e_2 \rightarrow 272^{LUMO}e_3$* |
| | 28% $261e_2 \rightarrow 272^{LUMO}e_3$* | | |
| 401 (0.008) | 32% $261e_2 \rightarrow 271^{LUMO}e_3$* | 400 (0.04) | 24% $268b_2 \rightarrow 271^{LUMO}e_3$* |
| | 31% $265e_2 \rightarrow 271^{LUMO}e_3$* | | 23% $263e_2 \rightarrow 271^{LUMO}e_3$* |
| | | | 22% $268b_2 \rightarrow 272^{LUMO}e_3$* |
| | | | 22% $263e_2 \rightarrow 272^{LUMO}e_3$* |
| 415 (0.09) | 50% $268b_2 \rightarrow 271^{LUMO}e_3$* | 404 (0.04) | 41% $268b_2 \rightarrow 271^{LUMO}e_3$* |
| | 32% $268b_2 \rightarrow 272^{LUMO}e_3$* | | 27% $268b_2 \rightarrow 272^{LUMO}e_3$* |
| | 23% $267a_1 \rightarrow 273e_1$ | | 20% $267a_1 \rightarrow 273e_1$ |
| 568 (0.45) [627] | 45% $269b_1 \rightarrow 271^{LUMO}e_3$* | 571 (0.51) [643] | 49% $269b_1 \rightarrow 272^{LUMO}e_3$* |
| | 29% $269b_1 \rightarrow 272^{LUMO}e_3$* | | 33% $270^{HOMO}a_2 \rightarrow 274e_1$* |
| | 22% $270^{HOMO}a_2 \rightarrow 273e_1$* | | 23% $268b_2 \rightarrow 271^{LUMO}e_3$* |
| 716 (0.04) [696] | 60% $270^{HOMO}a_2 \rightarrow 273e_1$* | 689 (0.014) | 50% $270^{HOMO}a_2 \rightarrow 274e_1$* |
| | 38% $269b_1 \rightarrow 271^{LUMO}e_3$* | | 38% $269b_1 \rightarrow 272^{LUMO}e_3$* |
| | | | 27% $270^{HOMO}a_2 \rightarrow 274e_1$* |

[a] The corresponding oscillator strength is given in parentheses; wavelengths given in brackets are experimental data observed by us. [b] The nature of the electronic transitions and percentage contribution of each transition are shown. Asterisks indicate antibonding orbitals.

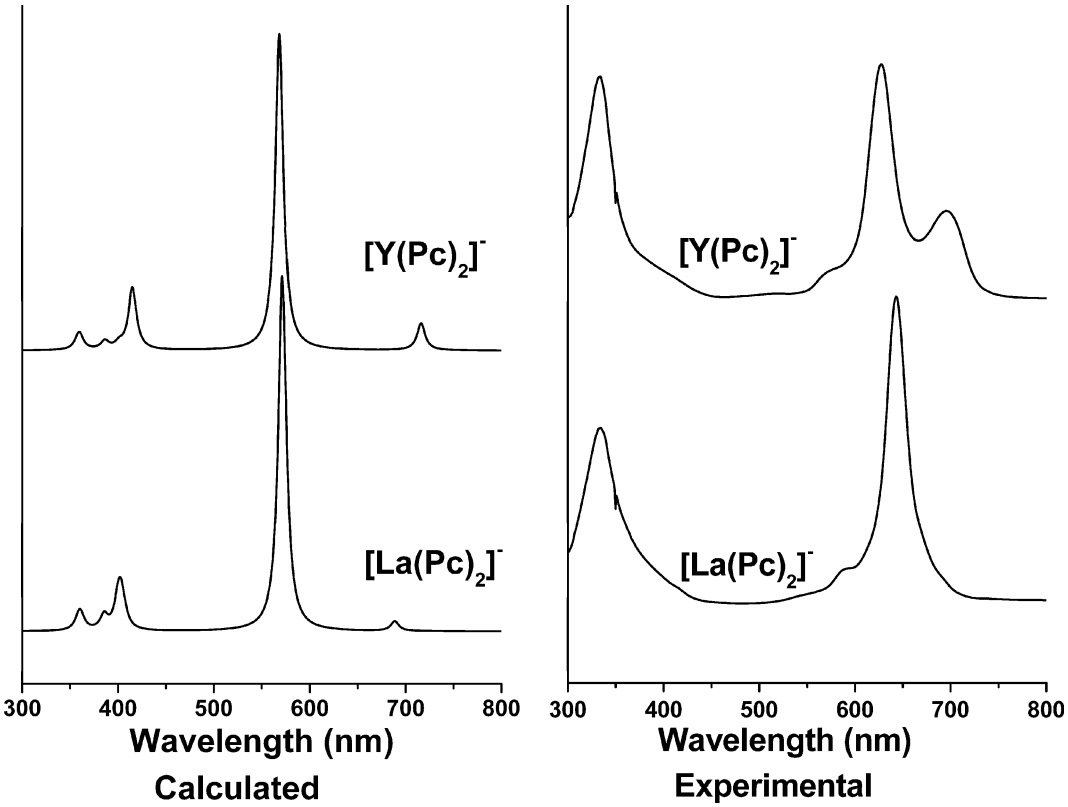


**Figure 4.** Calculated and experimental electronic absorption spectra of $[Y(Pc)_2]^-$ and $[La(Pc)_2]^-$.

from HOMO with $a_2$ symmetry to LUMO + 1 orbital (the second unoccupied orbital) with $e_1$ symmetry, while the former one at the shorter wavelength is mainly due to $\pi \rightarrow \pi^*$ electronic transition from HOMO − 1 ($b_1$ symmetry) to LUMO ($e_3$ symmetry).

It is worth noting that in the simulated electronic absorption spectrum of $[La(Pc)_2]^-$, Table 3, the weaker calculated Q-band at 689 nm in longer wavelength shows a blue shift and the stronger calculated Q-band at 571 nm at the shorter wavelength shows a red shift compared with those of $[Y(Pc)_2]^-$, leading to a decreased splitting between the two Q absorptions of $[La(Pc)_2]^-$ and indicating a decreased $\pi-\pi$ interaction between the two Pc rings in $[La(Pc)_2]^-$. This is in good accord with the experimental findings for several series of different bis-(phthalocyaninato) rare earth complexes,[31] and this trend can be well explained by studying the orbitals involved in these electronic transition. As described in the Molecular Orbitals section (Figure 2), the energy level of 270 $a_2$ orbital (HOMO) in $[La(Pc)_2]^-$ is lower than that in $[Y(Pc)_2]^-$, whereas the energy level of 269 $b_1$ orbital (HOMO − 1) of $[La(Pc)_2]^-$ is higher than that of $[Y(Pc)_2]^-$. This leads to a much smaller energy difference between 270 $a_2$ orbital and 269 $b_1$ orbital for

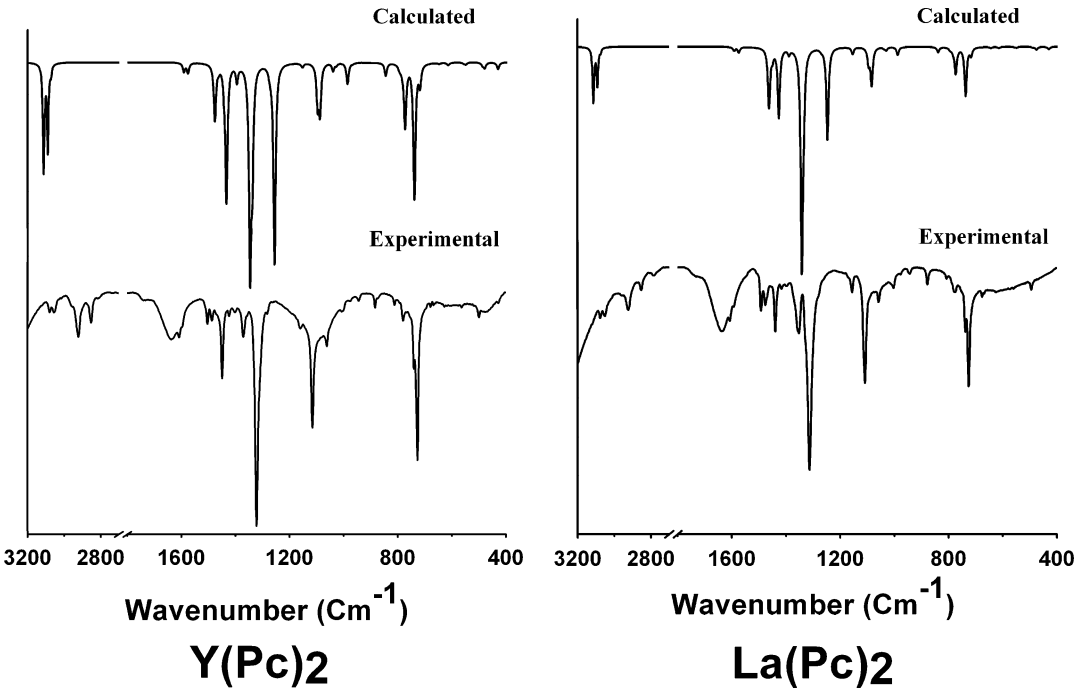


**Figure 5.** Comparison of the calculated and experimental IR spectra of $Y(Pc)_2$ and $La(Pc)_2$.

$[La(Pc)_2]^-$ than for $[Y(Pc)_2]^-$. Similarly, the energy difference between 271 $e_3$ orbital (LUMO) and 273 $e_1$ orbital (LUMO + 1) of $[La(Pc)_2]^-$ is also smaller compared with that of $[Y(Pc)_2]^-$. As a result, unlike the case of $[Y(Pc)_2]^-$, the two Q bands of $[La(Pc)_2]^-$ tend to appear at the same location. Actually, for $[La(Pc)_2]^-$, only one intense Q-band at 643 nm was observed experimentally due to the very narrow splitting and very weak intensity of the Q-band in the lower energy side.

It is noteworthy that, in spite of the same location of the B band of $[La(Pc)_2]^-$ at 359 nm with that of $[Y(Pc)_2]^-$, their origins are different. As mentioned above, this band for $[Y(Pc)_2]^-$ is mainly due to the $\pi \rightarrow \pi^*$ electronic transition from HOMO ($a_2$ symmetry) to the much higher unoccupied orbital (281 $e_1$ orbital), while for $[La(Pc)_2]^-$ mainly from the much lower occupied orbital (263 $e_2$ orbital) to LUMO + 1. This might be attributed to the fact that some electronic transition modes in the B band of $[Y(Pc)_2]^-$ are prohibited in $[La(Pc)_2]^-$ due to unsuitable orbital symmetry (vice versa).

**Infrared Spectra.** The calculated IR spectra of $M(Pc)_2$ (M = Y, La) together with their experimental ones are compared in Figure 5. As shown in Figure 5 (for further detail, see Table S2 of Supporting Information), the IR spectra of $M(Pc)_2$ (M = Y, La) obtained by calculation are in good accord with those recorded experimentally. Figure S4 (Supporting Information) gives the intuitional correspondence relationship of the calculated and experimental data by fitting them to a linear function. The slope of the line for $Y(Pc)_2$ is 1.012 and the intercept only 19, showing good consistency between the calculated and experimental data. Even better consistency than $Y(Pc)_2$ was found for $La(Pc)_2$, with the slope and the intercept being only 1.011 and 16, respectively. Good consistencies between the calculated and experimental IR spectra verify again the good performance of the B3LYP method and the LANL2DZ basis set used for these bis(phthalocyaninato) rare earth systems.

As expected, along with the decease of the ionic size from La to Y, all the absorption peaks in the IR spectrum of $Y(Pc)_2$ and $[Y(Pc)_2]^-$ show a blue shift compared with those of $La(Pc)_2$ and $[La(Pc)_2]^-$, respectively, due to enhanced inter-ring $\pi-\pi$ interaction (Figure 5; see also Figure S4, Supporting Information). However, the shift extent is different depending on the different vibration modes. The peaks whose vibration modes involve the contribution of central metal have been calculated to show larger extent of blue shift than those modes including only the Pc ring. This is reasonable since the peaks involving vibration modes of central metal are sensitive to the ionic size of central metal. For instance, the peak at 233 $cm^{-1}$ for $Y(Pc)_2$, contributed by the Y−N stretching with Y atom oscillating along the direction parallel to the two mean planes formed by the isoindole nitrogen atoms and coupled with the isoindole out-of-plane bending vibrations, takes a blue shift of more than 40 $cm^{-1}$ compared with the corresponding peak for $La(Pc)_2$. In contrast, the peak at 777 $cm^{-1}$ for $Y(Pc)_2$, which is due to the C−H out-of-plane bending vibration mode of the Pc ring according to our calculation, shows a blue shift of only ca. 2 $cm^{-1}$ compared with the corresponding peak for $La(Pc)_2$. Nevertheless, these calculated results are in line with the experimental findings.[32]

Also according to our calculations, the IR spectra of reduced $[M(Pc)_2]^-$ (M = Y, La) are somewhat different from those of neutral $M(Pc)_2$ (M = Y, La) due to the difference in the molecular structure and electronic state (Figure 5; see also Figure S4, Supporting Information). For instance, the typical vibration peaks of $Pc^{2-}$ due to the pyrrole stretching coupled with M−N stretching and C−H in-plane bending appearing at 1283 and 1273 $cm^{-1}$ for $[Y(Pc)_2]^-$ and $[La(Pc)_2]^-$, respectively, do not appear in the IR spectra of neutral $Y(Pc)_2$ and $La(Pc)_2$. In contrast, a very weak absorption peak is found in the corresponding range of IR spectra of reduced double-deckers, while the corresponding peak at 1258 and 1246 $cm^{-1}$ contributed from pyrrole stretching coupled with M−N stretching and C−H bending of Pc ligands appears even as the second strongest one in the IR spectrum for the neutral compounds $M(Pc)_2$ (M = Y, La), on the basis of the calculation results. These two absorptions appear to be good IR marker bands in distinguishing the neutral and reduced bis(phthalocyaninato) rare earth complexes.

The absorption peaks in the range of 1310−1350 $cm^{-1}$ are noticeable, and our calculated results give different assignments from the previous experimental identification. On the basis of

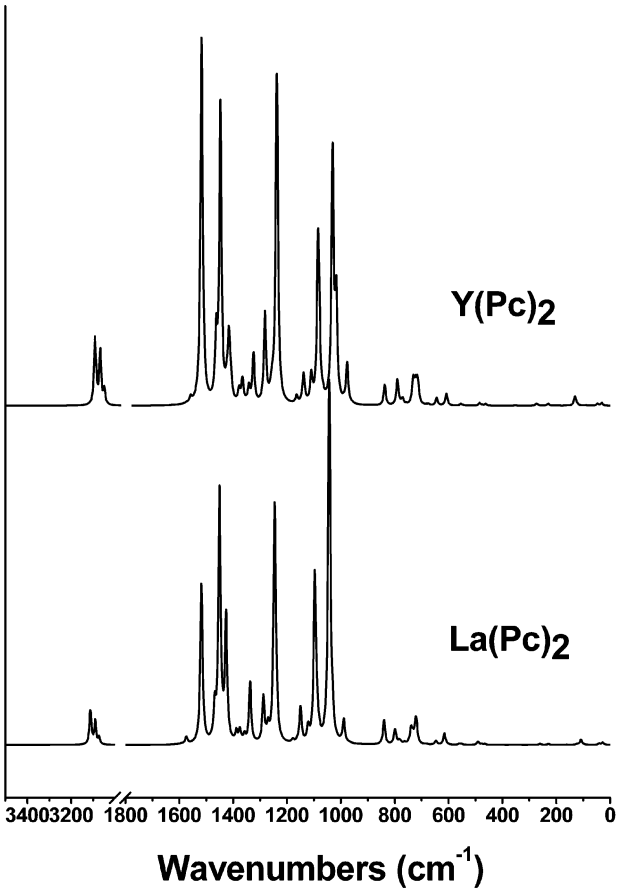


**Figure 6.** Simulated Raman spectra of $Y(Pc)_2$ and $La(Pc)_2$.

the research work of Kadish and co-workers[11,33] and by comparing the IR characteristics between $M^{III}(Pc)_2$ and $[NBu_4][M^{III}(Pc)_2]$,[27] the absorption band observed at 1310−1320 $cm^{-1}$ in the IR spectra of neutral bis(phthalocyaninato) rare earth(III) complexes $M^{III}(Pc)_2$ is attributed to the $Pc^{\bullet -}$ radical characteristic IR marker band, while that at ca. 1330 $cm^{-1}$ of the reduced form $[NBu_4][M^{III}(Pc)_2]$ is assigned to the $Pc^{2-}$ dianion characteristic IR marker band.[32c] As shown in Figure 5, the calculated peaks at 1348 and 1342 $cm^{-1}$ for $Y(Pc)_2$ and $La(Pc)_2$, respectively, should correspond with the experimentally observed absorptions at 1322 and 1313 $cm^{-1}$ in their IR spectra. Different from the previous assignment to the pyrrole stretching, however, normal coordinate analysis reveals that this absorption is due to the isoindole stretching coupled with C−H in-plane bending for the neutral bis(phthalocyaninato) rare earth(III) complexes $M(Pc)_2$ (M = Y, La) according to our calculations. Nevertheless, calculation results indicate that the reduced double-deckers $[M(Pc)_2]^-$ (M = Y, La) also show a similar absorption in the same region at 1341 and 1337 $cm^{-1}$ for $[Y(Pc)_2]^-$ and $[La(Pc)_2]^-$, respectively, also contributed by the isoindole stretching coupled with C−H in-plane bending (Figure 5; see also Figure S4 and Table S2, Supporting Information). These results, in combination with the fact that a similar absorption band is also observed in the IR spectra of divalent metal complexes of phthalocyanines,[17] suggest that the absorption peak near 1330 $cm^{-1}$ should also include typical vibration modes of $Pc^{2-}$. As a result, the recorded peak at 1322 and 1313 $cm^{-1}$ in the IR spectra of $Y(Pc)_2$ and $La(Pc)_2$, respectively, might be assigned as the hybrid vibration modes of $Pc^{\bullet -}$ and $Pc^{2-}$.

**Raman Spectra.** The simulated Raman spectra of $M(Pc)_2$ and $[M(Pc)_2]^-$ (M = Y, La) are displayed in Figure 6 and Figure S5 (Supporting Information), respectively, and corresponding data are listed in Table S3 (Supporting Information). As can be expected according to the IR spectra, our calculated Raman spectra also correspond well with the experimental ones.[32c,34] In line with the IR spectroscopic results, the scattering peaks in the calculated Raman spectra of both the neutral $Y(Pc)_2$ and reduced $[Y(Pc)_2]^-$ all locate at the higher-energy side of corresponding peaks of $La(Pc)_2$ and $[La(Pc)_2]^-$, due to enhanced ring−ring $\pi-\pi$ interaction of the Y compounds compared with the La counterparts, associated with the smaller ionic size of $Y^{3+}$ than $La^{3+}$. Also due to the difference in the electron state, there are somewhat different features in the Raman spectra of neutral $M(Pc)_2$ and reduced $[M(Pc)_2]^-$ (M = Y, La).

## Conclusion

An accurate description of the molecular structures, molecular orbitals, atomic charges, and UV−vis, IR, and Raman spectra of neutral bis(phthalocyaninato) rare earth(III) complexes $M(Pc)_2$ (M = Y, La) as well as their reduced products $[M(Pc)_2]^-$ (M = Y, La) has been provided by DFT and TDDFT calculations. The calculated results are in good agreement with the experimental data, indicating that the method and basis set selected are feasible for calculating such a large molecule as double-decker phthalocyaninato lanthanide complexes. It has been found that the ionic size of the central rare earth metal has more influence on the M−N bond length and inter-ring distance than on the structure parameters within the Pc rings in the double-decker molecules of both the neutral and reduced bis(phthalocyaninato) rare earth(III) complexes. Reduction of the neutral $M(Pc)_2$ into $[M(Pc)_2]^-$ induces the reorganization of their orbitals and charge distribution but very little change in their structure. The orbital energy level and orbital nature of the frontier orbitals are also described and explained in terms of atomic character. Due to the decreased $b_1-a_2$ (HOMO − 1 and HUMO) and $e_3-e_1$ (HUMO and HUMO + 1) orbital energy gap from $[Y(Pc)_2]^-$ to $[La(Pc)_2]^-$, the splitting of the two Q bands decreases from $[Y(Pc)_2]^-$ to $[La(Pc)_2]^-$. All the absorption peaks in the IR and Raman spectra of $Y(Pc)_2$ and $[Y(Pc)_2]^-$ show blue shifts compared with those of the lanthanum analogues due to the enhanced inter-ring $\pi-\pi$ interaction. The calculated peaks at 1283 and 1273 $cm^{-1}$ for $[Y(Pc)_2]^-$ and $[La(Pc)_2]^-$ and at 1258 and 1246 $cm^{-1}$ for $Y(Pc)_2$ and $La(Pc)_2$, respectively, can work as good IR marker bands in distinguishing the neutral and reduced bis(phthalocyaninato) rare earth complexes. The recorded peaks at 1322 and 1313 $cm^{-1}$ in the IR spectra of $Y(Pc)_2$ and $La(Pc)_2$, respectively, might be assigned as the hybrid vibration modes of $Pc^{\bullet -}$ and $Pc^{2-}$ instead of the mode of pure $Pc^{\bullet -}$ according to the previous experimental assignment.

**Acknowledgment.** Financial support from the Natural Science Foundation of China (Grants 20325105, 20431010, and 20501011), National Ministry of Science and Technology of China (Grant 2001CB6105-07), and Ministry of Education of China, Shandong University, is gratefully acknowledged. We are also grateful to the Shandong Province High Performance Computing Center for a grant of computer time.

**Supporting Information Available:** Assignments of all calculated IR and Raman spectra, compared with experimental data; simulated IR and Raman spectra of $[M(Pc)_2]^-$ (M = Y, La); α molecular orbital map of $Y(Pc)_2$; and atomic composition data. This material is available free of charge via the Internet at http://pubs.acs.org.

## References and Notes

(1) (a) Leznoff, C. C.; Lever, A. B. P. *Phthalocyanine: Properties and Applications*; VCH: New York, 1989−1996; Vols. 1−4. (b) McKeown, N. B. *Phthalocyanines Materials: Synthesis, Structure and Function*; Cambridge University Press: New York, 1998. (c) Kadish, K. M.; Smith, K. M.; Guilard, R. *The Porphyrin Handbook*; Academic Press: San Diego, CA, 2000−2003; Vols. 1−20.

(2) Jiang, J.; Kasuga, K.; Arnold, D. P. In *Supramolecular Photosensitive and Electroactive Materials*; Nalwa, H. S., Ed.; Academic Press: New York, 2001; Chapt. 2, pp 113−210.

(3) Ng, D. K. P.; Jiang, J. *Chem. Soc. Rev.* **1997**, *26*, 433.

(4) (a) Komatsu, T.; Ohta, K.; Fujimoto, T.; Yamamoto, I. *J. Mater. Chem.* **1994**, *4*, 533. (b) Jones, R.; Krier, A.; Davidson, K. *Thin Solid Films* **1997**, *298*, 228.

(5) (a) Madru, M.; Guillaud, G.; Al Sadoun, M.; Maitrot, M.; Clarisse, C.; Le Contellec, M.; André, J.-J.; Simon, J. *Chem. Phys. Lett.* **1987**, *142*, 103. (b) Madru, R.; Guillaud, G.; Al Sadoun, M.; Maitrot, M.; André, J.-J.; Simon, J.; Even, R. *Chem. Phys. Lett.* **1988**, *145*, 343. (c) Clarisse, C.; Riou, M. T.; Gauneau, M.; Le Contellec, M. *Electron. Lett.* **1988**, *24*, 674. (d) Guillaud, G.; Al Sadoun, M.; Maitrot, M.; Simon, J.; Bouvet, M. *Chem. Phys. Lett.* **1990**, *167*, 503.

(6) (a) Souto, J.; Rodríguez, M. L.; Desaja, J. A.; Aroca, R. *Int. J. Electron.* **1994**, *76*, 763. (b) Bassoul, P.; Toupance, T.; Simon, J. *Sens. Actuators, B* **1995**, *26*−*27*, 150. (c) Rickwood, K. R.; Lovett, D. R.; Lukas, B.; Silver, J. *J. Mater. Chem.* **1995**, *5*, 725. (d) Liang, B.; Yuan, C.; Wei, Y.; Zhang, Y.; Jiang, D.; Zhang, S.; Lu, A. *Synth. Met.* **1997**, *88*, 219. (e) Álvarez, J.; Souto, J.; Rodríguez-Méndez, M. L.; de Saja, J. A. *Sens. Actuators, B* **1998**, *48*, 339.

(7) Guéna, M.; Wu, Z. Y.; L'Her, M.; Pondaven, A.; Cadiou, C. *Appl. Phys. Lett.* **1998**, *72*, 765.

(8) Konami, H.; Hatano, M.; Kobayashi, N.; Osa, T. *Chem. Phys. Lett.* **1990**, *165*, 397.

(9) Buchler, J. W.; Hammerschmitt, P.; Kaufeld, I.; Löffler, J. *Chem. Ber.* **1991**, *124*, 2151.

(10) Chabach, D.; Tahiri, M.; De Cian, A.; Fischer, J.; Weiss, R.; El Malouli Bibout, M. *J. Am. Chem. Soc.* **1995**, *117*, 8548.

(11) Guilard, R.; Barbe, J.-M.; Ibnlfassi, A.; Zrineh, A.; Adamian, V. A.; Kadish, K. M. *Inorg. Chem.* **1995**, *34*, 1472.

(12) Buchler, J. W.; Scharbert, B. *J. Am. Chem. Soc.* **1988**, *110*, 4272.

(13) (a) Ishikawa, N.; Ohno, O.; Kaizu, Y.; Kobayashi, H. *J. Phys. Chem.* **1992**, *96*, 8832. (b) Ishikawa, N.; Ohno, O.; Kaizu, Y. *J. Phys. Chem.* **1993**, *97*, 1004. (c) Ishikawa, N.; Kaizu, Y. *J. Phys. Chem. A.* **2000**, *104*, 10009. (d) Ishikawa, N.; Sugita, M.; Okubo, T.; Tanaka, N.; Iino, T.; Kaizu, Y. *Inorg. Chem.* **2003**, *42*, 2440. (e) Ishikawa, N. *J. Porphyrins Phthalocyanines* **2001**, *5*, 87.

(14) Sénéchal-David, K.; Hemeryck, A.; Tancrez, N.; Toupet, L.; Williams, J. A. G.; Ledoux, I.; Zyss, J.; Boucekkine, A.; Guégan, J.-P.; Le Bozec, H.; Maury, O. *J. Am. Chem. Soc.* **2006**, *128*, 12243.

(15) (a) Lee, C.; Yang, W.; Parr, R. G. *Phys. Rev. B* **1988**, *37*, 785. (b) Becke, A. D. *J. Chem. Phys.* **1993**, *98*, 5648.

(16) (a) Gong, X.; Xiao, H.; Tian, H. *J. Mol. Struct. (THEOCHEM)* **2002**, *593*, 93. (b) Liao, M.; Kar, T.; Gorun, S. M.; Scheiner, S. *Inorg. Chem.* **2004**, *43*, 7151. (c) Day, P. N.; Wang, Z. Q.; Pachter, R. *J. Mol. Struct. (THEOCHEM)* **1998**, *455*, 33.

(17) (a) Zhang, Y.; Zhang, X.; Liu, Z.; Bian, Y.; Jiang, J. *J. Phys. Chem. A* **2005**, *109*, 6363. (b) Zhang, Y.; Zhang, X.; Liu, Z.; Xu, H.; Jiang, J. *Vib. Spectrosc.* **2006**, *40*, 289.

(18) Petit, L.; Adamo, C.; Russo, N. *J. Phys. Chem. B* **2005**, *109*, 12214.

(19) Liu, X.; Xu, L. C.; He, T. J.; Chen, D. M.; Liu, F. C. *Chem. Phys. Lett.* **2003**, *379*, 517.

(20) Hay, P. J.; Wadt, W. R. *J. Chem. Phys.* **1985**, *82*, 299.

(21) Dunning, T. H., Jr.; Hay, P. J. In *Modern Theoretical Chemistry*; Schaefer, H. F., III, Ed.; Plenum: New York, 1976; Vol. 3, p 1.

(22) Tian, W. Q.; Ge, M.; Gu, F. L. L.; Yamada, T.; Aoki, Y. *J. Phys. Chem. A* **2006**, *110*, 6285.

(23) Paillaud, J. L.; Drillon, M.; Decian, A.; Fisher, J.; Weiss, R.; Poinsot, R.; Herr, A. *Physica B* **1991**, *175*, 337.

(24) Peng, C.; Ayala, P. Y.; Schlegel, H. B.; Frisch, M. J. *J. Comput. Chem.* **1996**, *17*, 49.

(25) NIST Computational Chemistry Comparison and Benchmark Database, NIST Standard Reference Database, Number 101, Release 10, May 2004; Johnson, R. D., III, Ed.; http://srdata.nist.gov/cccbdb.

(26) Frisch, M. J.; Trucks, G. W.; Schlegel, H. B.; Scuseria, G. E.; Robb, M. A.; Cheeseman, J. R.; Montgomery, Jr., J. A.; Vreven, T.; Kudin, K. N.; Burant, J. C.; Millam, J. M.; Iyengar, S. S.; Tomasi, J.; Barone, V.; Mennucci, B.; Cossi, M.; Scalmani, G.; Rega, N.; Petersson, G. A.; Nakatsuji, H.; Hada, M.; Ehara, M.; Toyota, K.; Fukuda, R.; Hasegawa, J.; Ishida, M.; Nakajima, T.; Honda, Y.; Kitao, O.; Nakai, H.; Klene, M.; Li, X.; Knox, J. E.; Hratchian, H. P.; Cross, J. B.; Bakken, V.; Adamo, C.; Jaramillo, J.; Gomperts, R.; Stratmann, R. E.; Yazyev, O.; Austin, A. J.; Cammi, R.; Pomelli, C.; Ochterski, J. W.; Ayala, P. Y.; Morokuma, K.; Voth, G. A.; Salvador, P.; Dannenberg, J. J.; Zakrzewski, V. G.; Dapprich, S.; Daniels, A. D.; Strain, M. C.; Farkas, O.; Malick, D. K.; Rabuck, A. D.; Raghavachari, K.; Foresman, J. B.; Ortiz, J. V.; Cui, Q.; Baboul, A. G.; Clifford, S.; Cioslowski, J.; Stefanov, B. B.; Liu, G.; Liashenko, A.; Piskorz, P.; Komaromi, I.; Martin, R. L.; Fox, D. J.; Keith, T.; Al-Laham, M. A.; Peng, C. Y.; Nanayakkara, A.; Challacombe, M.; Gill, P. M. W.; Johnson, B.; Chen, W.; Wong, M. W.; Gonzalez, C.; Pople, J. A. Gaussian 03, Revision B.05; Gaussian, Inc.: Pittsburgh, PA, 2003.

(27) Hückstädt, H.; Tuta, A.; Göldner, M.; Cornelissen, U.; Homborg, H. *Z. Anorg. Allg. Chem.* **2001**, *627*, 485.

(28) Ostendorp, G.; Homborg, H. *Z. Naturforsch. B* **1995**, *50*, 1200.

(29) Haghighi, M. S.; Franken, A.; Homborg, H. *Z. Naturforsch. B* **1994**, *49*, 812.

(30) Zhu, P.; Lu, F.; Pan, N.; Arnold, D. P.; Zhang, S.; Jiang, J. *Eur. J. Inorg. Chem.* **2004**, 510.

(31) Kobayashi, N. *Coord. Chem. Rev.* **2002**, *227*, 129.

(32) (a) Jiang, J.; Arnold, D. P.; Yu, H. *Polyhedron* **1999**, *18*, 2129. (b) Lu, F.; Bao, M.; Ma, C.; Zhang, X.; Arnold, D. P.; Jiang, J. *Spectrochim. Acta, Part A* **2003**, *59*, 3273. (c) Jiang, J.; Bao, M.; Rintoul, L.; Arnold, D. P. *Coord. Chem. Rev.* **2006**, *250*, 424.

(33) Kadish, K. M.; Moninot, G.; Hu, Y.; Dubois, D.; Ibnlfassi, A.; Barbe, J.-M.; Guilard, R. *J. Am. Chem. Soc.* **1993**, *115*, 8153.

(34) (a) Jiang, J.; Rintoul, L.; Arnold, D. P. *Polyhedron* **2000**, *19*, 1381. (b) Bao, M.; Wang, R.; Rintoul, L.; Liu, Q.; Arnold, D. P.; Ma, C.; Jiang, J. *Polyhedron* **2006**, *25*, 1195.